Molecular view of the Rayleigh-Taylor instability in compressible Brownian fluids

A. Wysocki[*] and H. Löwen[†]

Institut für Theoretische Physik II,

Heinrich-Heine-Universität Düsseldorf,

Universitätsstraße 1, D-40225 Düsseldorf, Germany

Abstract

The onset of the Rayleigh-Taylor instability is studied a compressible Brownian Yukawa fluid mixture on the "molecular" length and time scales of the individual particles. As a model, a two-dimensional phase-separated symmetric binary mixture of colloidal particles of type A and B with a fluid-fluid interface separating an A-rich phase from a B-rich phase is investigated by Brownian computer simulations when brought into non-equilibrium via a constant external driving field which acts differently on the different particles and perpendicular to the interface. Two different scenarios are observed which occur either for high or for low interfacial free energies as compared to the driving force. In the first scenario for high interfacial tension, the critical wavelength λ_c of the unstable interface modes is in good agreement with the classical Rayleigh-Taylor formula provided dynamically rescaled values for the interfacial tension are used. The wavelength λ_c increases with time representing a self-healing effect of the interface due to a local density increase near the interface. The Rayleigh-Taylor formula is confirmed even if λ_c is of the order of a molecular correlation length. In the second scenario for very large driving forces as compared to the interfacial line tensions, on the other hand, the particle penetrate easily the interface by the driving field and form microscopic lanes with a width different from the predictions of the classical Rayleigh-Taylor formula. The results are of relevance for phase-separating colloidal mixtures in a gravitational or electric field.

PACS numbers: 05.70.Ln, 05.70.Np, 82.70.Dd, 05.40.Jc

---

[*]Electronic address: adam@thphy.uni-duesseldorf.de

[†]Electronic address: hlowen@thphy.uni-duesseldorf.de

I. INTRODUCTION

Interface instabilities in driven non-equilibrium systems are well-known from macroscopic hydrodynamics [1, 2]. Examples include the classic Rayleigh-Taylor instability [1] of a heavy liquid on top of another lighter liquid, the Mullins-Sekerka fingering instability [3, 4] in diffusive systems and the Saffmann-Taylor instability [5, 6] for compressed liquids of different viscosities. However, what is much less clear is the microscopic origin of these instabilities, i.e. a view which resolves the microscopic discrete particle trajectories causing the instability. Recently there has been progress in simulating large systems with 10000-10000000 of discrete particles forming an interface [7, 8, 9, 10]. In particular, the microscopic origin of the Rayleigh-Taylor instability was explored in huge molecular dynamics [7, 9, 10] and direct numerical [8] computer simulations. A natural question concerns the applicability of coarse-grained hydrodynamics towards microscopic spatial dimensions. The basic quantities entering in hydrodynamics auch as the viscosity or the surface tension are quantities which are only defined for large systems and exhibit finite-size corrections when applied to small inhomogeneities.

Another approach to interfacial instabilities is via mesoscopic colloidal suspensions which bear the fascinating possibility to study the particle trajectories in real-space by video microscopy in quasi-two-dimensional suspensions [11]. Well-characterized colloidal suspensions serve as model systems for many questions of many-body systems [12, 13] including interfaces [14, 15, 16, 17, 18, 19]. The strength of an external field is easily tunable for colloids in striking contrast to molecular liquids. The dynamics of the mesoscopic colloidal particles which are embedded in a microscopic solvent is Brownian rather than Newtonian [20] such that dynamical quantities are different. To the best of our knowledge, for compressible Brownian fluids nothing is known about the onset of the Rayleigh-Taylor instability on a length scale of interparticle distances. Clearly, it will be different from molecular dynamics where heat will be generated and inertia effects can lead to turbulence [7, 9, 10]. One promising investigation in the Newtonian case is for a suspension of heavy granular grains where Rayleigh-Taylor instabilities have recently been observed by Rehberg and coworkers [21, 22] but also in this work the individual particle trajectories were not resolved. Mixtures of colloids and polymers with a real-space analysis of the colloids trajectories represent another valuable system to look at for interfacial instabilities in external driving fields [14].

In the present paper we study, by Brownian dynamics computer simulations, the particle-resolved onset of the Rayleigh-Taylor instability. In our model, an interface separating an A-rich from an A-poor fluid is exposed to an external field which acts differently on the different particles and is directed perpendicular to the interface. In order to keep the model simple [23] and to link to two-dimensional colloidal suspensions, we take two spatial dimensions and a symmetric equimolar mixture interacting via a Yukawa pair potential. Most of our characteristics, however, will carry over to three-dimensional systems, to asymmetric mixtures, and to different interparticle interactions.

The external field is so large that it will induce local density inhomogeneities such that the fluid is compressible in contrast to the ordinary case treated within the Navier-Stokes equations [10]. We observe two different scenarios which occur either for high or for low interfacial free energies as compared to a typical thermal energy per average particle distance. In the first scenario for high interfacial tension, an interfacial instability is observed which is driven by the competition of the cost in interfacial tension versus gain in potential energy, similar in spirit to the classical Rayleigh-Taylor instability. The classical threshold value for the wavelength of unstable interface perturbations is confirmed provided the line tension is dynamically rescaled in terms of the actual local density at the interface. The critical wavelength separating stable from unstable density undulations increases with time. This can be interpreted as a "self-healing effect" of the interface caused by a local density increase near the interface. In the second scenario for small interfacial tensions, on the other hand, the particle penetrate easily the interface by the driving field and form microscopic lanes similar to previous simulation studies [24, 25, 26, 27, 28]. In this case the classical threshold for the unstable wavelength is smaller than a molecular correlation length such that a breakdown of macroscale hydrodynamics is expected. Our results are of relevance for phase-separating colloidal mixtures in a gravitational or electric field where similar effects have recently been reported by Aarts and coworkers [14] and for settling granular grains [21].

The paper is organized as follows: In section II, we define the model used and describe briefly our simulation technique. As a prerequisite, a microscopic calculation of the density profile and the line tension is presented in section III. We further review the classical Rayleigh-Taylor instability briefly in section IV. Results for the interface instability for high line tensions are presented in section V, while the case of small line tensions is described in section VI. Conclusion are given in section VII. In particular, we discuss a possible

verification of our predictions in experiments.

II. THE MODEL

In our model [25], we consider a symmetric binary colloidal mixture comprising $N = N_A + N_B$ Brownian colloidal particles in $d = 2$ spatial dimensions. The particles are in an area S with a fixed total number density of $\rho = \frac{N}{S}$. Half of them are particles of type A, the other half is of type B with partial number density $\rho_A = \rho_B = \frac{\rho}{2}$. The colloidal suspension is held at fixed temperature T via the bath of microscopic solvent particles. The colloidal particles of species a and b ($a, b \in \{A, B\}$) are interacting via an effective Yukawa pair potential

$$\frac{V_{ab}(r)}{k_B T} = U_0 \, \sigma_{ab} \, \frac{\exp\left[-\kappa(r - \sigma_{ab})/\sigma\right]}{r}, \tag{1}$$

Here r is the center-to-center separation, $k_B T$ is the thermal energy, U_0 is a dimensionless amplitude, σ is the particle diameter as a length scale and κ is the inverse screening length. The set of diameters σ_{ab} is taken as

$$\sigma_{AA} = \sigma_{BB} = \sigma \tag{2}$$

$$\sigma_{AB} = \sigma(1 + \Delta) \tag{3}$$

We chose $\Delta > 0$ corresponding to positive non-additivity. This implies that the cross-interaction $V_{AB}(r)$ is more repulsive than $V_{AA}(r) = V_{BB}(r)$, which drives phase separation into an A-rich and a B-rich phase.

The dynamics of the colloidal particles is overdamped Brownian motion. The friction constant $\xi = 3\pi\eta\sigma$ (with η denoting the shear viscosity of the solvent) is assumed to be the same for both A and B particles. The constant external force for the ith particle of species a, $\vec{F}_i^{(a)}$, is acting differently on the both constituents of the binary mixture. It is $\vec{F}_i^{(A)} = \vec{e}_z F$ for A particles and $\vec{F}_i^{(B)} = -\vec{e}_z F$ for B particles. The stochastic Langevin equations for the colloidal trajectories $\vec{r}_i^{(a)}(t)$ with $i = 1, ..., N_a$ ($a \in \{A, B\}$) read as

$$\xi \frac{d\vec{r}_i^{(a)}}{dt} = \sum_{\substack{j=1 \\ j \neq i}}^{N_a} \vec{F}_{ij}^{(aa)} + \sum_{j=1}^{N_b} \vec{F}_{ij}^{(ab)} + \vec{F}_i^{(a)} + \vec{F}_i^{(R)}(t). \tag{4}$$

where

$$\vec{F}_{ij}^{(ab)} = -\vec{\nabla}_{\vec{r}_i^{(a)}} V_{ab}(r_{ij}^{(ab)}), \qquad (5)$$

$r_{ij}^{(ab)} = \mid \vec{r}_i^{(a)} - \vec{r}_j^{(b)} \mid$, and b is the complementary index to a ($b = A$ if $a = B$ and $b = B$ if $a = A$). The right-hand-side includes all forces acting onto the colloidal particles, namely the force resulting from inter-particle interactions, the external constant force, and the random forces $\vec{F}_i^{(R)}$ describing the collisions of the solvent molecules with the ith colloidal particle. The latter are Gaussian random numbers with zero mean, $\overline{\vec{F}_i^{(R)}} = 0$, and variance

$$\overline{(\vec{F}_i^{(R)})_\alpha(t)(\vec{F}_j^{(R)})_\beta(t')} = 2k_B T \xi \delta_{\alpha\beta} \delta_{ij} \delta(t - t'). \qquad (6)$$

The subscripts α and β stand for the two Cartesian components. In the absence of an external field and for $\Delta = 0$, the model reduces to a two-dimensional Brownian Yukawa fluid in equilibrium which has been extensively investigated as far as structural and dynamical equilibrium correlations and freezing transitions are concerned [29, 30, 31]. For a positive Δ and vanishing external drive, our system will lead to equilibrium fluid-fluid phase separation including a critical point which has been studied in non-additive hard-core models by theory and simulation, see e.g. Ref. [32, 33, 34, 35, 36, 37].

We solve the Langevin equations of motion by Brownian dynamics simulations (BD) [38, 39, 40] using a finite time-step Δt and the technique of Ermak [41, 42]. The typical size of the time-step was $0.003\tau_B$, where $\tau_B = \xi\sigma^2/V_0$ is a suitable Brownian timescale. As a reference, the field-free case $\vec{F} = 0$ is studied extensively first. This is an equilibrium situation. In the simulation set-up here, we put $N_A = 1000$ A and $N_B = 1000$ B particles into a rectangular cell of lengths L in x-direction and D in z-direction with $\frac{D}{L} = \frac{8}{5}$ such that the total colloidal number density is $\rho = \frac{N}{DL}$. Then the system spontaneously exhibits a fluid-fluid interface along the x-direction separating an A-rich from a B-rich fluid provided the density is larger than the critical density. To have an single interface system, without disturbing effects due to external walls, periodic boundary conditions are used in the x-direction while antiperiodic boundary conditions are used in z-direction. With antiperiodic boundary conditions, the particle type is changed from A to B if an A particle is crossing a boundary in z-direction and vice versa. In a finite slab around this boundary, all interactions are set to be equal, i.e. the cross interaction is $V_{AB} = V_{AA} = V_{BB}$. This avoids a second interface and minimizes finite-size effects. Similar boundary condition shave been employed to study interfaces of symmetric polymer mixtures by Müller, Binder and coworkers [43].

5

We equillibrated 3×10^5 time steps corresponds to an equilibration time of $900\tau_B$ and gathered statistics again for a further simulation time of $900\tau_B$. We also checked that our data do not suffer from finite size effects by choosing a larger system with $N_A = 4000$ A and $N_B = 4000$ B particles with $\frac{D}{L} = \frac{3}{5}$. The antiperiodic boundary conditions force the interface to be parallel to the x-axis. All our investigations in nonequilibrium are with this larger system size.

With an equilibrated interface as a starting configuration we suddenly turn on the external field which drives the particles against the interface. An interface instability was observed. 300 different equilibrated starting configuration were then typically used in order to perform time-dependent averages. For our nonequilibrium simulations, the antiperiodic boundary conditions in z direction has no consequences once the particles are driven against the interface.

III. DENSITY PROFILES AND EQUILIBRIUM FLUID-FLUID INTERFACIAL FREE ENERGY

In equilibrium, a phase-separated binary fluid mixture is characterized by its z-dependent partial density profiles $\rho_A(z)$ and $\rho_B(z)$ as defined via

$$\rho_a(z) = \left\langle \sum_{i=1}^{N_a} \delta(z - z_i^{(a)}) \right\rangle \tag{7}$$

where $a \in \{A, B\}$ and $\langle \ldots \rangle$ denotes a canonical average. Furthermore the associated fluid-fluid interfacial free energy γ is a key quantity. Since our model is two-dimensional, this interfacial free energy γ corresponds to a line tension. In a symmetric binary mixture, the partial density profiles and the line tension γ depend on the temperature and the total number density ρ.

Obviously, due to the A-B symmetry of our model, the density profiles are symmetric, i.e. $\rho_A(z) = \rho_B(-z)$, if the interface position is at $z = 0$. Computer simulation results of the density profiles for a strong positive nonadditivity $\Delta = 1.6$ and various bulk densities at a fixed temperature are presented in Figure 1. For high densities one clearly idenfifies a depletion zone in the interface as generated by the large non-additivity. For densities closer to the critical one, however, the density profiles are getting flatter and particles interpenetrate mutually. For large bulk densities, a slight density oscillation shows up as typical for fluid

6

interfaces when the Fisher-Widom line is exceeded [44]. Clearly, for the parameters chosen, the mixture is almost completely phase-separated, i.e. the partial densities of the A particles is practically zero in the B-region and vice-versa. Again this is different very close to the critical point.

We have also calculated the equilibrium line tension as a function of density for fixed temperature by using "exact" computer simulation techniques. The interfacial free energy can be gained by integration of the anisotropy of the pressure tensor [45, 46, 47, 48, 49]. In two spatial dimensions, this expression reads

$$\gamma = \int\limits_{-\infty}^{\infty} [P_N(z) - P_T(z)] \, dz \tag{8}$$

where $P_N(z) = p_{zz}(z)$ and $P_T(z) = p_{xx}(z)$ are the diagonal components of the local pressure tensor. This local pressure tensor has the following form [50, 51, 52, 53, 54]

$$p_{\alpha\beta}(z) = (\rho_A(z) + \rho_B(z))k_B T \delta_{\alpha\beta}$$
$$-\frac{1}{L}\left\langle \sum_{\substack{1 \leq i < j \leq N_a \\ a=A,B}} \left(\vec{r}_{ij}^{(aa)}\right)_\alpha \left(\vec{F}_{ij}^{(aa)}\right)_\beta \frac{1}{\left|z_{ij}^{(aa)}\right|} \Theta\left(\frac{z - z_i^{(a)}}{z_{ij}^{(aa)}}\right) \Theta\left(\frac{z_j^{(a)} - z}{z_{ij}^{(aa)}}\right)\right.$$
$$\left. + \sum_{\substack{1 \leq i \leq N_A \\ 1 \leq j \leq N_B}} \left(\vec{r}_{ij}^{(AB)}\right)_\alpha \left(\vec{F}_{ij}^{(AB)}\right)_\beta \frac{1}{\left|z_{ij}^{(AB)}\right|} \Theta\left(\frac{z - z_i^{(A)}}{z_{ij}^{(AB)}}\right) \Theta\left(\frac{z_j^{(B)} - z}{z_{ij}^{(AB)}}\right)\right\rangle \tag{9}$$

where the subscripts α and β stand for the two Cartesian components, $\vec{r}_{ij}^{(ab)} = \vec{r}_i^{(a)} - \vec{r}_j^{(b)}$, $z_{ij}^{(ab)} = z_i^{(a)} - z_j^{(b)}$ and $\Theta(z)$ is the Heaviside step function. The z-dependence of the anisotropy of the pressure tensor is plotted in Figure 1 as well. As can be deduced from Figure 1, its main weight is centered in the interface position around $z = 0$. The oscillations of the density field for high densities correlate to that of the pressure tensor.

Simulation results for the density-dependent line tension $\gamma(\rho)$ for two different nonadditivities $\Delta = 0.8$ and $\Delta = 1.6$ are presented in Figure 2. Most of our calculations were for parameter combinations well away from the critical point where the line tension is mainly governed by internal energy such that the anisotropy of the pressure tensor is significant resulting in a relative small statistical error for γ, see Figure 2a. Some further points are also for smaller densities closer to the critical point, see Figure 2b. By crudely extrapolating the data one could estimate the critical density to be at $\rho_c \sigma^2 \approx 0.08$ for $\Delta = 0.8$ and

$\rho_c \sigma^2 \approx 0.04$ for $\Delta = 1.6$ as indicated by arrows in Figure 2b. This extrapolation was cross-checked by mapping our Yukawa system onto that of effective non-additive hard disks using the prescription of Barker-Henderson for the effective hard-core diameter [55]. The critical point can then be read off from that of a non-additive symmetric hard disk binary mixture which has been studied in detail via theory and simulation by Giaquinta and coworkers [36]. We find good agreement with our extrapolation as compared to the mapping procedure. As can be further deduced from Figure 2, the line tension $\gamma(\rho)$ is strongly increasing with density. This is expected as a density increase means a smaller spacing between A and B particles such that the energetic non-additivity is getting more pronounced. At fixed density and temperature, the line tension increases with Δ which is clearly due to the fact that a larger nonadditivity leads to a larger energy cost of different particle species meeting at the interface.

IV. CLASSICAL RAYLEIGH-TAYLOR INSTABILITY

The classical Rayleigh-Taylor instability is obtained for a heavy incompressible liquid on top of a lighter incompressible liquid [1, 56]. A small harmonic interfacial undulation with a wave length λ yields a favorable decrease in potential energy but at the same time a free energy penalty due to the increasing arc length of the interface which costs line tension. If the wave length is larger than a critical one $\lambda > \lambda_c$, however, the penalty is smaller than the gain such that an unstable mode whose amplitude grows in time is present. The critical wave length can be calculated in our two-dimensional situation as

$$\lambda_c = \frac{2\pi}{k_c} = 2\pi \sqrt{\frac{\gamma}{\left|\vec{F}^{(A)} - \vec{F}^{(B)}\right|\rho}} \tag{10}$$

where γ is the line tension as introduced in the previous section. Since the concept of line tension is a macroscopic one, Eq.(10) is only justified as long as λ_c is much larger than any microscopic distance as e.g. the mean interparticle spacing $a = \frac{1}{\sqrt{\rho}}$. This requires that the line tension has to be much larger than the driving force difference

$$\lambda_c \gg a \quad \Rightarrow \quad \gamma \gg \left|\vec{F}^{(A)} - \vec{F}^{(B)}\right| \tag{11}$$

In the opposite limit

$$\gamma \ll \left|\vec{F}^{(A)} - \vec{F}^{(B)}\right| \tag{12}$$

it is expected that the classical concept of the Rayleigh-Taylor instability will break down. We shall explore this case in detail in section VI. Another question concerns the applicability of the Rayleigh-Taylor instability criterion when λ_c is of a similar order than the mean interparticle spacing a. As we shall show below, the criterion works remarkable well even if λ_c is close to a.

V.   RESULTS FOR HIGH AND MODERATE INTERFACIAL TENSIONS

Typical snapshots of our nonequilibrium computer simulations are presented in Figure 3 for 4 different times and for two different densities $\rho^* = \rho\sigma^2 = 0.2, 0.4$ and two different strengths of the driving force $F^* = F\sigma/k_BT = 10, 40$. The parameter combinations investigated and the corresponding ratios of the line tension γ and the driving force F are summarized in Table I. They are of the order 1 (for combination A-C) or a bit smaller (for combination D) such that the Rayleigh-Taylor instability wavelength is larger than or of the order of the mean interparticle spacing a, see again Table I for the ratio λ_c/a. We call an interface tension "high" if $\lambda_c/a > 1$ and "intermediate" if $\lambda_c/a \approx 1$. This is in contrast to the case of low surface tensions (combination E) where λ_c/a is significantly smaller than 1 which is studied in chapter VI.

The system was started with an equilibrated single interface situation. The initial interface is pretty smooth but carries capillary fluctuations on it. The density depletion shown in Figure 1, manifests itself as a clear void region in the interface reminiscent of a "forest-aisle" which is induced by the strong energy cost when two different particle species do meet.

Then instantaneously the external driving forces were turned on forcing the particles to drift against each other. This first causes a local density increase close to the interface. Then interface undulations are getting more pronounced deforming the flat interface. This is the most efficient channel for different particle species to reverse their height. A typical characteristic undulation wave length can be identified from the simulation snapshot which we shall quantify later. Furthermore nonlinear effects such as interfacial overhangs ("mushrooms") can be seen (e.g. in Figure 3a for the largest time) until the mixture penetrates through eachother and the height reversal is complete.

In order to quantify the structural signatures of the interface instability further, we consider the Fourier transform of the interface position as a function of time. In detail, let

$h(x, t)$ be the interface position of a given configuration at a time t, and

$$\tilde{h}(k, t) = \int_0^L h(x, t) \exp(-ikx) \, dx \tag{13}$$

the corresponding Fourier transform. We are interested in the time dependence of the averaged power spectral density which is defined as

$$P(k, t) = \langle \tilde{h}(k, t) \tilde{h}^*(k, t) \rangle \tag{14}$$

where $\langle \ldots \rangle$ now denotes an ensamble average over inital equilibrated configurations which dynamically evolved after a time t. If, at a given t, $P(k, t)$ possesses a sharp maximum at $k = k_m$, this implies that the interface will exhibit mainly undulations with a wave length of $\lambda_m = 2\pi/k_m$.

As an aside, let us remark that an alternative way of obtaining the line tension γ is via the equilibrium capillary wave spectrum $P(k, t = 0)$ which behaves as

$$P(k, t = 0) = \frac{k_B T}{\gamma} \frac{L}{k^2} \tag{15}$$

for small wave vectors k [53, 57, 58]. We have checked that values for the line tension γ as obtained from this formula are consistent with those obtained from Eq.(8).

We are now in a position to define a differential growth rate $\Gamma(k, t)$ via

$$\Gamma(k, t) = \frac{1}{P(k, t)} \frac{d}{dt} P(k, t) \tag{16}$$

A positive sign of $\Gamma(k, t)$ implies that a mode of wave number k is growing at a time t while a negative sign means that - at a given time t - the mode is decreasing.

In detail, the following numerical procedure was used to obtain the actual interface position $h(x, t)$: For a given particle configuration at time t, we construct Voronoi cells around each particle and define the interface based on the associated Voronoi polygons. The polygon vertices that belong to cells of particles of both species A and B define a set of M^* non-equidistant co-ordinates $(h_n, x_n)_{n=1,\ldots,M^*}$. Now we eliminate the protuberance in the interface profile to get an functional interrelation for $h(x)$. For further analysis we interpolate $(h_n, x_n)_{n=1,\ldots,M^*}$ by a cubic spline and eliminate sharp bends by using a simple low-pass filter

$$h_n \to h_n^* = (h_n + h_{n+1})/2 \tag{17}$$

10

where $n = 1, \ldots, M$ and $h_{M+1} \equiv h_1$. This procedure results in a unique z-position $h(x, t)$ of the interface at a given time t.

Results for the differential growth rate $\Gamma(k, t)$ are shown in Figure 4 as a contour plot in the plane spanned by the time t and the wave vector k. As in Figure 3, data for the four different parameters combinations A-D are presented. The white **zero line** summarizes points where $\Gamma(k, t)$ vanishes and separates two regimes with growing (stable) modes and damped (unstable) wave numbers. Although this line is noisy, it can be read off from Figure 4 that there is a whole band of wave numbers which are growing after an induction time of roughly τ_B. The lower limit of unstable wave numbers is significantly larger than the inverse simulation box length, while its upper limit is always smaller than a microscopic wave number of the order of $2\pi/a$. Between these two boundaries, roughly at the arithmetic mean of the two limits, there is a wave number with a **maximal** growth rate. !! The first basic observation is that for parameter combinations A-C where λ_c/a is larger than 1 the upper limit of unstable wave numbers is *decreasing* with time. !! This has to do with our equilibrated starting configuration. When the external field is turned on, there is a sedimentation-like process towards the interface which yields a local density increase at the interface. This behaviour can directly be seen in the simulation snapshots of Figure 3. Thereby the interface is getting stiffer as a fuction of time. We call this important effect *self-healing* of the interface, i.e. as a function of time the interface is getting less vulnerable with respect to short wavelength undulations. A possible destruction of the interface is efficiently blocked by a density accumulation. It is tempting to correlate this to an effective interface tension with a scaled density as obtained e.g. by the maximal total density ρ_m close to the interface. This maximal density ρ_m is a function of time. If one plugs this time-dependent density into the expression for $\gamma(\rho)$, one obtains a dynamically rescaled Rayleigh-Taylor expression (9). The corresponding wave number is also shown in Figure 4, see the open circles with error bars. Clearly the basic effect is encaptured by the dynamical rescaling as the classical Rayleigh-Taylor unstable wave number coincides well with the upper unstable limit. The agreement is in particular encouraging for parameter combinations A-C where $\lambda_c/a > 1$.

A special remark is in order for parameter combination D where λ_c is of the order of a. In fact, we estimate a microscopic wave number by $2\pi\sqrt{\rho_m}$ and data for this wave vector $2\pi\sqrt{\rho_m}$ are included in Figure 4 as crosses. Even in this case, the comparison between

11

the upper unstable wave number and the scaled Rayleigh-Taylor prediction is qualitative. This implies that the classic Rayleigh-Taylor criterion is astonishingly robust even close to molecular spacings.

On the other hand, the **maximal** growth rate is seen as light region for small wave vectors. This wave number is slightly decreasing with time as well. We have further compared the wave number of maximal growth by calculating the second maximum of the height-height-correlation function which is defined as

$$C(k,t) = \left\langle h(x,t)h(x + \frac{2\pi}{k},t) \right\rangle \qquad (18)$$

The position of the second maximum of $C(k,t)$ is also included as a square-line in Figure 4. It is increasing as a function of time towards larger wave numbers, i.e. smaller wave lengths. The increase is small and confined to a small "induction time" of the process. We attribute this to an initial process which has to do with the fact that due to the non-homogeneous capillary wave spectrum Eq.(15), undulations with larger wave lengths have initially a larger amplitude and have therefore more weight in $C(k,t)$. This gives rise to the crossover to higher wave number after an induction time which is pretty sharp for the parameter combinations A and B.

Finally we note that at higher k the growth rate is getting positive for larger times. This is due to the fact that the interface position is no longer sinoidal but starts to exhibit sharp parts close to overhangs. This is turn will generate higher Fourier modes to grow and this is what is indicated by the zero-line at higher k and larger times.

We finally think that the zero-line at high k and smaller times (in Figure 4a and 4b) is statistical noise. Furthermore, a full comparison of the differential growth rates to a hydrodynamic approach [1] requires a dynamically scaled viscosity and is left for future studies.

VI. RESULTS FOR LOW INTERFACIAL TENSIONS

Similar computer simulations were done as in the previous section but now in the regime where the line tension was low in the sense of the criterion of Eq.(12) such that λ_c was significantly smaller than a. Simulation snapshots are shown for $\rho^* = 0.075$ close to the estimated critical density in Figure 5. In this case, the interface is penetrable by the strongly

driven particles and $\gamma/F = 0.002$ and $\lambda_c/a = 0.2$, see the parameter combination E in Table I.

In penetrating the interface, the particles form lanes similar to the behaviour in additive mixtures in Refs. [25, 26]. The width of the lanes is comparable to the correlation length of the mixture meaning that single worms of particles are formed [27]. At the head of the lanes both spikes and extrusions are visible. A similar behaviour is found for even smaller densities below the critical density where the system is mixed in equilibrium. Hence the Rayleigh-Taylor criterion would predict a submolecular unstable wave length but the actual realized instability wavelength is a molecular correlation length of the system of the order of a.

VII.   CONCLUSIONS

In conclusion, we have studied the onset of the Rayleigh-Taylor interface instability on length scales of interparticle distances for a compressible Brownian fluid mixture. Depending on the equilibrium interfacial tension, either a direct transition towards lane formation or the macroscopic Rayleigh-Taylor instability was found. An interesting dynamical effect is the self-healing mechanism for the interface which is produced by a density accumulation of particles driven against eachother which then causes an increase of the instability wavelength as a function of time.

It would be interesting to study the dynamical process of phase separation by starting from a completely mixed system under the influence of the driving forces. Here one would expect a subtle interplay between phase separation kinetics which typically results in fractals and lane formation [59]. One should further investigate more extensively the dependence on the "sedimentation height", i.e. how the data are affected by a larger initial D in z-direction perpendicular to the interface. Moreover. it would be interesting to start the simulation by impressing a prescribed wave length as an interface undulation and checke its differential growth. A third set-up for another initial configuration which is typically used for the molecular dynmics simulations [10] would be to equilibrate first with respect to the external field with a fixed interface as induced e.g. by a thin hard platelet separating the two fluid phases. The effects of different starting configuration on the onset of the Rayleigh-Taylor instability will be left for future studies.

For simplicity, all our simulations were done in two spatial dimensions. In three dimensions, similar effects should persist. However, the characteristic wavelength has now two components parallel to the interface. The self-stabilizing effect of the interface and the two extreme limits should be similar as in two dimensions. The lane formation, for instance, has also be shown to be present in three spatial dimensions.

Let us finally discuss some possible experimental verifications. Strongly non-additive mixtures which phase-separate into two fluid phases are found in colloid/polymer mixtures which exhibit colloid-rich and colloid-poor fluid phases for size ratio of about 0.5 or larger between the polymer and the colloid [60]. Recently a phase-separating mixture of colloids and polymers was observed in sedimentation by Aarts and coworkers [17]. In particular, it was observed that large regions of phase-separated colloid-rich and colloid-poor phases exhibit a transition towards lane formation. The characteristic wavelength is of the order of that given by the Rayleigh-Taylor instability Eq.(10) [61]. A full quantitative comparison has still to be performed. Another system were such lane formation has been seen and which could be a candidate for a quantitative comparison is a xanthan-colloid mixture [62]. Finally we mention the fascinating possibility to study the mixture of complex plasmas involving dust grains for interface instability in real space [63, 64].

[1] S. Chandrasekhar, *Hydrodynamic and Hydromagnetic Stability* (Oxford University Press, 1961).

[2] M. C. Cross and P. C. Hohenberg, Rev. Mod. Physics **65**, 851 (1993).

[3] J. Ignes-Mullol and P. Oswald, Phys. Rev. E **61**, 3969 (2000).

[4] I. Cantat, K. Kassner, C. Misbah, and H. Müller-Krumbhaar, Phys. Rev. E **58**, 6027 (1998).

[5] A. Lindner, D. Bonn, E. C. Poire, M. Ben Amar, and J. Meunier, J. Fluid Mechanics **469**, 237 (2002).

[6] P. Coussot, J. Fluid Mechanics **380**, 363 (1999).

[7] W. Alda, W. Dzwinel, J. Kitowski, J. Moscinski, M. Pogoda, and D. A. Yuen, Computers in Physics **12**, 595 (1998).

[8] T. W. Pan, D. D. Joseph, and R. Glowinski, J. Fluid Mechanics **434**, 23 (2001).

[9] W. Dzwinel and D. A. Yuen, International Journal of Modern Physics C **12**, 91 (2001).

[10] K. Kadau, T. C. Germann, N. G. Hadijconstantinou, G. Denionte, P. S. Lomdahl, B. L. Holian, and B. J. Alder, to be published.

[11] C. A. Murray and D. H. van Winkle, Phys. Rev. Letters **58**, 1200 (1987).

[12] P. N. Pusey, in *Liquids, Freezing and the Glass Transition*, edited by J. P. Hansen, D. Levesque, and J. Zinn-Justin (North Holland, Amsterdam, 1991).

[13] H. Löwen, J. Phys: Condensed Matter **13**, R415 (2001).

[14] E. H. A. de Hoog, W. K. Kegel, A. van Blaaderen, and H. N. W. Lekkerkerker, Phys. Rev. E **64**, 021407 (2001).

[15] J. M. Brader, R. Evans, M. Schmidt, and H. Löwen, J. Phys.: Condensed Matter **14**, L1 (2002).

[16] K. P. Velikov, C. G. Christova, R. P. A. Dullens, and A. van Blaaderen, Science **296**, 106 (2002).

[17] D. G. A. L. Aarts, J. H. van der Wiel, and H. N. W. Lekkerkerker, J. Phys.: Condensed Matter **15**, S245 (2003).

[18] J. P. Hoogenboom, A. K. van Langen-Suurling, J. Romijn, and A. van Blaaderen, Phys. Rev. Lett. **90**, 138301 (2003).

[19] J. P. Hoogenboom, A. Yethiraj, A. K. van Langen-Suurling, J. Romijn, and A. van Blaaderen,

Phys. Rev. Lett. **89**, 256104 (2002).

[20] H. Löwen, J. P. Hansen, and J. N. Roux, Phys. Rev. A **44**, 1169 (1991).

[21] C. Völtz, W. Pesch, and I. Rehberg, Phys. Rev. E **65**, 011404 (2001).

[22] C. Völtz, Phys. Rev. E **68**, 021408 (2003).

[23] C. Reichhardt, C. J. Olson-Reichhardt, and M. B. Hastings, cond-mat **0308097** (2003).

[24] D. MacGowan and D. J. Evans, Phys. Rev. A **34**, 2133 (1986).

[25] J. Dzubiella, G. P. Hoffmann, and H. Löwen, Phys. Rev. E **65**, 021402 (2002).

[26] J. Dzubiella and H. Löwen, J. Phys.: Condensed Matter **14**, 9383 (2002).

[27] J. Chakrabarti, J. Dzubiella, and H. Löwen, Europhys. Letters **61**, 415 (2003).

[28] H. Löwen and J. Dzubiella, Faraday Discussions **123**, 99 (2003).

[29] H. Löwen, J. Phys.: Condens. Matter **4**, 10105 (1992).

[30] B. Löhle and R. Klein, Physica A **235**, 224 (1997).

[31] K. J. Naidoo and J. Schnitker, J. Chem. Phys. **100**, 3114 (1994).

[32] V. Ehrenberg, H. M. Schaink, and C. Hoheisel, Physica A **169**, 365 (1990).

[33] P. Nielaba, Int. J. Thermophys **17**, 157 (1996).

[34] E. Lomba, M. Alvarez, L. Lee, and N. Almarza, J. Chem. Phys. **104**, 4180 (1996).

[35] M. Al-Naafa, J. B. El-Yakubu, and E. Z. Hamad, Fluid Phase Equilibr. **154**, 33 (1999).

[36] F. Saija and P. V. Giaquinta, J. Chem. Phys. **117**, 5780 (2002).

[37] W. T. Góźdź, J. Chem. Phys. **119**, 3309 (2003).

[38] H. Löwen and G. Hoffmann, Phys. Rev. E **60**, 3009 (1999).

[39] G. P. Hoffmann and H. Löwen, J. Phys.: Condensed Matter **13**, 9197 (2001).

[40] H. Löwen, J. P. Hansen, and J. N. Roux, Phys. Rev. A **44**, 1169 (1991).

[41] M. P. Allen and D. J. Tildesley, *Computer simulations of liquids* (Oxford University Press, 1987).

[42] D. L. Ermak, J. Chem. Phys **62**, 4189 (1975).

[43] A. Werner, F. Schmid, M. Müller, and K. Binder, J. Chem. Phys. **107**, 8175 (1997).

[44] R. Evans and A. J. Archer, Phys. Rev. E **64**, 041501 (2001).

[45] J. G. Kirkwood and F. P. Buff, J. Chem. Phys. **17**, 338 (1949).

[46] B. Smit, Phys. Rev. A **37**, 3431 (1988).

[47] J. Alejandre, D. J. Tildesley, and G. A. Chapela, J. Chem. Phys. **102**, 4574 (1995).

[48] R. B. Pandey, A. Milchev, and K. Binder, Macromolecules **30**, 1194 (1997).

16

[49] A. Milchev and K. Binder, J. Chem. Phys. **114**, 8610 (2001).

[50] J. H. Irving and J. G. Kirkwood, J. Chem. Phys. **18**, 817 (1950).

[51] S. Ono and S. Kondo, in *Encyclopedia of Physics*, edited by S. Flügge (Springer, Berlin, 1960).

[52] P. Schofield and J. H. Henderson, Proc. R. Soc. London A **379**, 231 (1982).

[53] J. S. Rowlinson and B. Widom, *Molecular Theory of Capillarity* (Oxford University Press, 1982).

[54] J. P. R. B. Walton, D. J. Tildesley, J. S. Rowlinson, and J. R. Henderson, Molecular Physics **48**, 1357 (1983).

[55] J. P. Hansen and I. R. McDonald, *Theory of Simple Liquids* (Academic Press Limited, 1990), 2nd ed.

[56] D. H. Sharp, Physica D **12**, 3 (1984).

[57] F. P. Buff, R. A. Lovett, and F. H. Stillinger, Phys. Rev. Lett. **15**, 621 (1965).

[58] J. D. Weeks, J. Chem. Phys. **67**, 3106 (1977).

[59] H. Löwen, C. N. Likos, R. Blaak, S. Auer, V. Froltsov, J. Dzubiella, A. Wysocki, and H. M. Harreis, in *Proceedings of the 3rd International Symposium on Slow Dynamics 2003*, edited by M. Tokuyama and I. Oppenheim (AIP Series, Sendai, 2003).

[60] M. Dijkstra, J. M. Brader, and R. Evans, J. Phys.: Condensed Matter **11**, 10079 (1999).

[61] D. G. A. L. Aarts, private communication.

[62] G. H. Koenderink, D. G. A. L. Aarts, V. W. A. Villeneuve, A. P. Philipse, R. Tuinier, and H. N. W. Lekkerkerker, Biomacromolecules **4**, 129 (2003).

[63] G. E. Morfill, H. M. Thomas, U. Konopka, and M. Zuzic, Physics of Plasmas **6**, 1769 (1999).

[64] P. K. Shukla, M. Torney, R. Bingham, and G. E. Morfill, Physica Scripta **67**, 350 (2003).

FIGURE AND TABLE CAPTIONS

Figure 1: Averaged density profiles $\rho_A(z)$ and $\rho_B(z)$ of the two particle species and anisotropy $P_N - P_T$ of the pressure tensor as a function of the distance z perpendicular to the interface for $\Delta = 1.6$ and for four different densities: $\rho\sigma^2 = 0.4$ (solid lines), $\rho\sigma^2 = 0.3$ (dashed lines), $\rho\sigma^2 = 0.2$ (dot-dashed line) and $\rho\sigma^2 = 0.15$ (short-dashed lines).

Figure 2: Reduced line tension $\gamma\sigma/k_B T$ as a function of reduced bulk density $\rho\sigma^2$ for two different nonadditivities $\Delta = 0.8$ (solid line) and $\Delta = 1.6$ (dot-dashed line). (a) Away from the critical point. (b) Closer to the critical point. The estimate for the critical density are shown as arrows.

Figure 3: Typical simulation snapshot for an interface in nonequilibrium with an external drive. There is a sharp interface between an A-rich and a B-rich fluid phase. The starting configuration was an equilibrated interface at $z = 0$. Four different times are shown as given in the legend. a) $\rho\sigma^2 = 0.2$ and $F^* = F\sigma/k_B T = 10$, b) $\rho\sigma^2 = 0.2$ and $F^* = F\sigma/k_B T = 40$, c) $\rho\sigma^2 = 0.4$ and $F^* = F\sigma/k_B T = 10$, d) $\rho\sigma^2 = 0.4$ and $F^* = F\sigma/k_B T = 40$.

Figure 4: Contour plots of the growth rate $\Gamma(k, t)$. Zero growth is shown by the white line. The rescaled classical Rayleigh-Taylor wave length $2\pi/\lambda_c$ is shown by the circles. Here is time-dependent maximum ρ_m of the total density at the interface is used. The statistical error stems from the uncertaincy of this density. The position of the second maximum in the height-height correlation function are the squares. The corresponding microscopic wave number as defined by $2\pi\rho_m^{1/2}$ and gives an estimate for the threshold to where a microscopic length scale are realized.
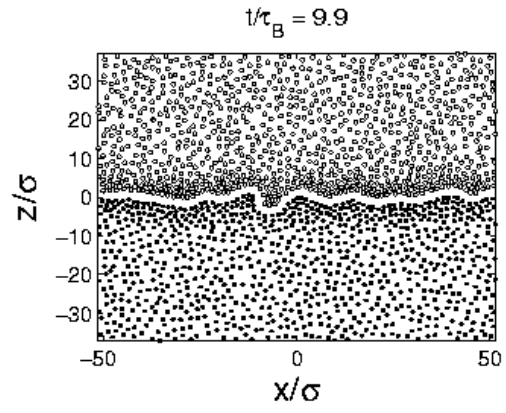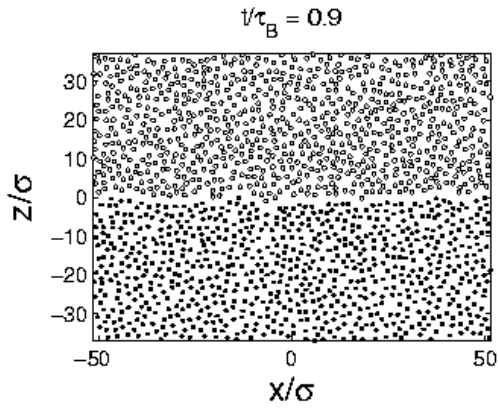
Figure 5: Typical simulation snapshot for an interface in nonequilibrium with an external drive. There is a sharp interface between an A-rich and a B-rich fluid phase. The starting configuration was an equilibrated interface at $z = 0$. Four different times are shown as given in the legend. The parameters are $\rho\sigma^2 = 0.075$ and $F^* = F\sigma/k_B T = 80$.
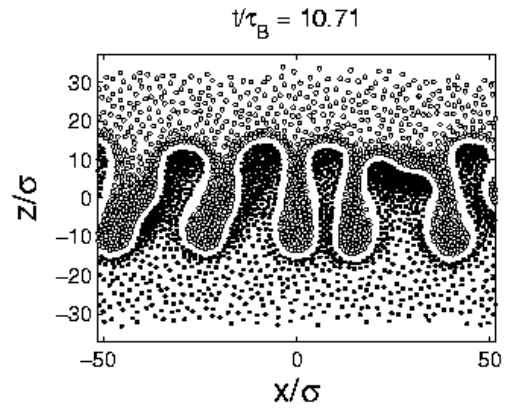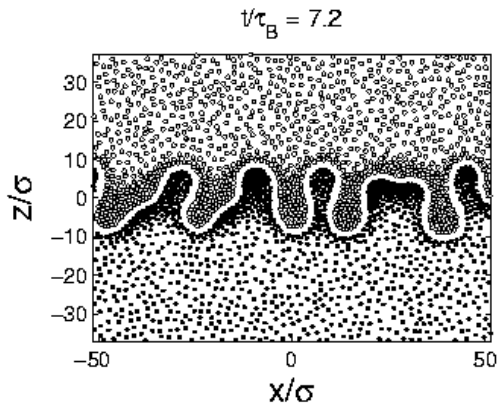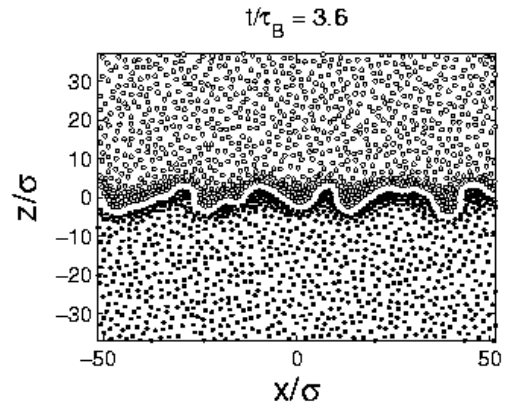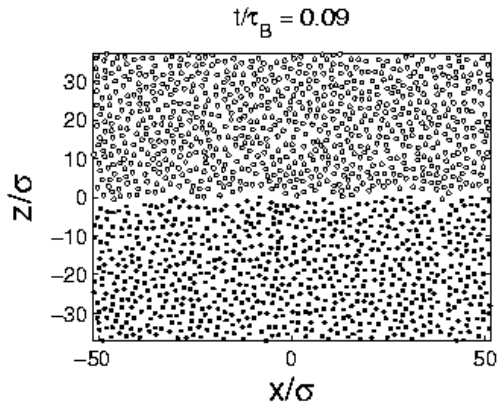
Table 1: Summary of the 5 parameters combinations studied in the paper. The corresponding ratios γ/F and λ_c/a are also given.
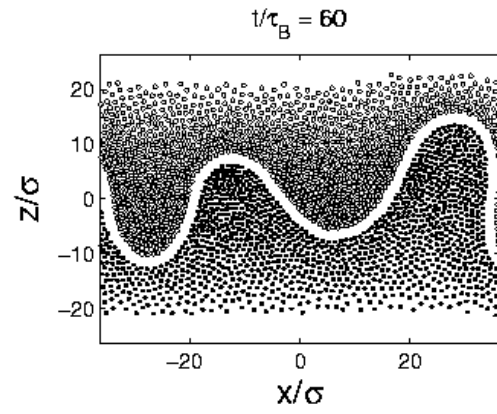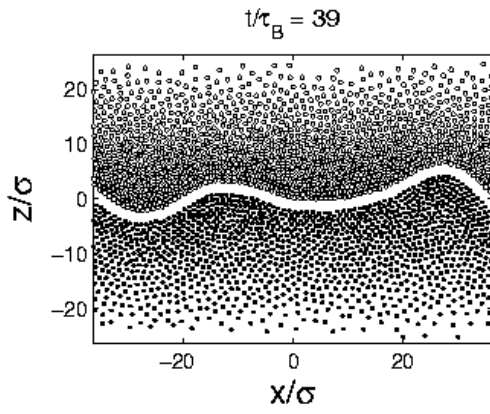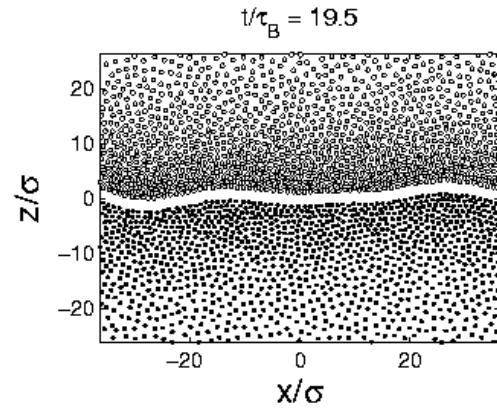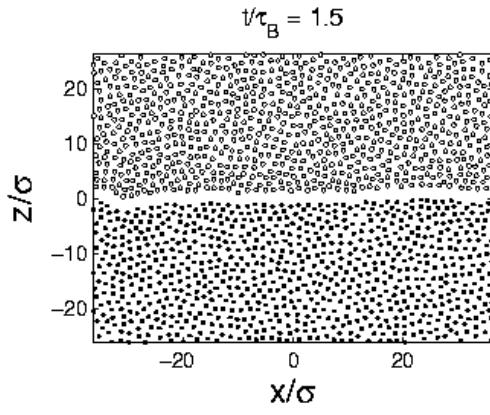
	ρ^*	F^*	γ/F	λ_c/a
A	0.4	10	1.3	5
B	0.4	40	0.32	2.5
C	0.2	10	0.2	2
D	0.2	40	0.05	1
E	0.075	80	0.002	0.2

$t/\tau_B = 0.09$ $t/\tau_B = 3.6$

$t/\tau_B = 7.2$ $t/\tau_B = 10.71$

$t/\tau_B = 0.3$

$t/\tau_B = 3$

$t/\tau_B = 6$

$t/\tau_B = 9$

25

$$\rho^*_{t=0} = 0.2, \; F^* = 40$$

$\Gamma(k,t)$

$\rho^{*}_{t=0} = 0.4, F^{*} = 10$

$\Gamma(k,t)$

$k = 2\pi/\lambda$

t/τ_{B}

$\rho^*_{t=0} = 0.4, F^* = 40$

$k = 2\pi/\lambda$

t/τ_B

$\Gamma(k,t)$

$t/\tau_B = 0.12$

$t/\tau_B = 1.68$

$t/\tau_B = 3.36$

$t/\tau_B = 4.8$